A-PDF Split DEMO : Purchase from www.A-PDF.com to remove the watermark

28. Detection of Low-Frequency Earthquakes in the non-volcanic tremor beneath the San Andreas Fault: a prospective tool for investigating deep fault dynamics?

Andrea Cannata (University of Catania), Margaret Hellweg, Robert M. Nadeau, Stefano Gresta (University of Catania)

28.1 Introduction

Non-volcanic tremor (NVT) has been observed in Cascadia, in southwest Japan and along the San Andreas Fault (*Schwartz and Rokosky*, 2007). In southwest Japan, the NVT is accompanied by relatively energetic and isolated pulses that have been identified as low-frequency earthquakes (LFEs; *Shelly et al.*, 2006). Compared with nearby ordinary earthquakes with similar amplitudes, LFEs are enriched in low frequencies (1-5 Hz). These events occur almost exclusively as part of an extended tremor signal (*Shelly et al.*, 2006). The analysis of such events allows the source of tremor to be tracked with good resolution in time and space, providing the capability of monitoring slow slip with good precision as it migrates along the subduction zone (*Shelly et al.*, 2007). Episodes of NVT along the San Andreas Fault (*Nadeau and Dolenc*, 2005) occur less often, are shorter and release less energy than those in the subduction zones. The aim of this work is to develop a detection procedure for LFEs in the NVT recorded along the San Andreas Fault in 2006-2007. In fact, the study of these events could contribute to significantly improving our knowledge of the deep dynamics of the San Andreas fault.

28.2 Data and Detection Methods

In this work the seismic signals recorded by the High-Resolution Seismic Network (HRSN; Figure 2.64a; see Chapter 3, Section 4.) were used. The analysis was applied to seismic signals from 48 NVT tremor episodes. Data windows start about 10 minutes before the beginning of the NVT and stop about 10 minutes after they end, giving a total of approximately about 30 hours.

To verify that the channels work and to highlight the frequency band characterised by the highest energy during the NVT episodes, the seismic signal was analysed using a Fast Fourier Transform (FFT). The tremor time series was divided into windows about 16 s long. The spectrum was calculated for each window (overlapping by 8 s) with a frequency resolution of 0.06 Hz. Then, the time development of the spectrum and its average were calculated for each tremor episode. Amplitudes were highest in the frequency band from 2 to 8 Hz, if signals below 2 Hz are excluded, where the signal to noise ratio is low and the sensor response drops off. Based on this result we decided to analyse this frequency band.

The detection method is divided into two steps, trigger detection and trigger selection.

Trigger detection

Trigger detection was based on three STA/LTA algorithms (short time average over long time average), each of which evaluates the ratio between short- and long-term energy density (squared data to facilitate combining multi-channel data in a Pythagorean sense) to find amplitude transients (*Withers et al.*, 1998). The first, the standard STA/LTA, was applied to three narrow frequency bands 2-4, 4-6 and 6-8 Hz, producing three lists of triggers. Because the optimal lengths of the windows depend on the frequency content of the seismic signal, the lengths of the short and long windows were chosen to be 3 and 27 times the center period of the frequency band analysed, respectively. Moreover, in this first method the data window is rectangular. In the second algorithm, the adaptive standard STA/LTA, the entire 2-8 Hz band was analysed. As an estimator of the dominant peak frequency, needed to adaptively calculate the length of the short and long windows, the moving average of the instantaneous frequency over 1.5 s was used, and the data window was also rectangular. Finally, in the third algorithm, the adaptive recursive STA/LTA, the data were windowed using a decaying exponential. The frequency band analysed was 2-8 Hz and the window lengths were calculated adaptively, as in the second algorithm.

Using these three algorithms we obtained 5 lists of triggers for each station. Then, by sliding 10-second-long moving windows over the lists for all stations, groups of triggers common at more than two stations were formed. Thus, we obtained 5 lists of common triggers from 5 lists of triggers for each station.

Trigger Selection

Because the signals that we are looking for have small amplitudes, the STA/LTA thresholds were set to low values. Obviously, the lower this threshold is, the less "reliable" are the triggers obtained. Therefore, two selection criteria were used to retain only "reliable" triggers. The first was based on the number of stations: only the triggers common at least at "N" stations were taken into account. The second consisted of evaluating the consistency of the time distribution of the common triggers with the locations of the stations: we plotted longitude and latitude of the stations and trigger time in the x, y and z axes, respectively; then, we determined the best fit plane, the one minimizing the perpendicular distances

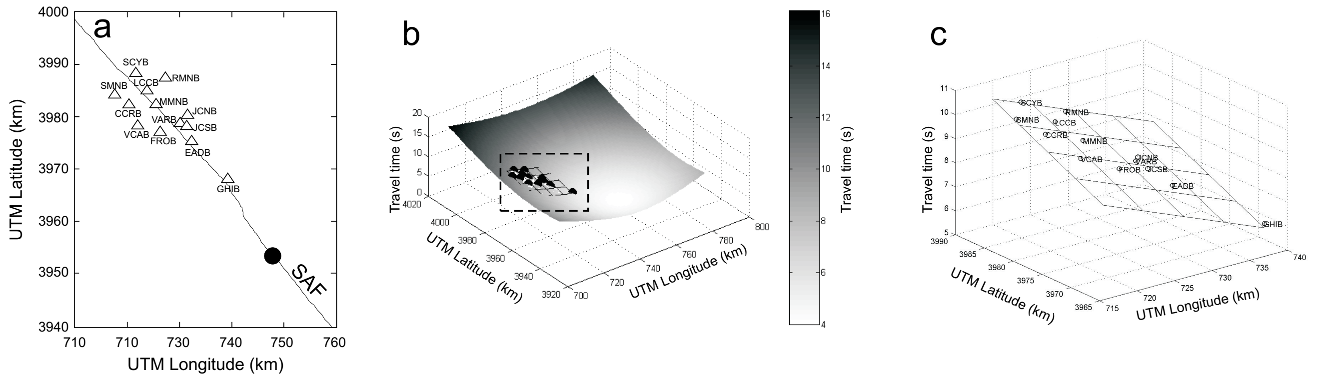

Figure 2.64: (a) Map showing the locations of the 13 stations belonging to the HRSN (triangles), a portion of the San Andreas Fault (SAF) and the epicentre of the theoretical source (black dot). (b) Distribution of the theoretical travel times (surface) and the fitting plane (grid plane) obtained taking into account only the 13 points corresponding to the stations (black dots); the dashed rectangle shows the portion of the plot highlighted in (c). (c) Theoretical travel times at the considered stations (black circles) and fitting plane (grid plane). See text for details.

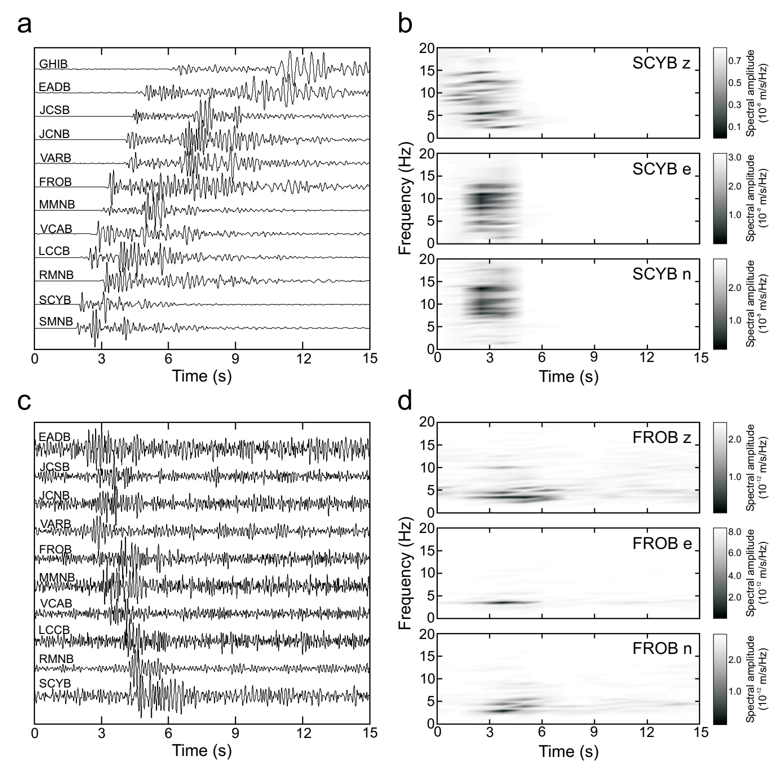

Figure 2.65: (a) Vertical component velocity recorded on January 30, 2006 (filter: 2-8 Hz) and (b) velocity spectrograms of the three components at SCYB. (c) Velocity signal of one of the horizontal component recorded on April 30, 2006 (filter: 2-8 Hz) and (d) velocity spectrograms of the three components at FROB.

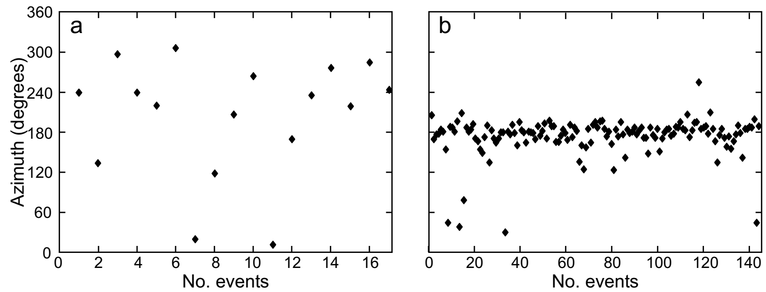

Figure 2.66: Azimuth values of the events of (a) group 1 and (b) group 2, obtained by using the plunge of the fitting plane.

from the stations, and calculated the residuals. Therefore, the triggers common at least at "N" stations were considered "reliable" if the sum of the rectified residuals was lower than a certain threshold, called "E". Obviously, this method is valid only if the source is far away from the station network; the tremor source location reported in *Nadeau and Dolenc* (2005) supports this assumption. By this fitting plane we were also able to roughly calculate an azimuth value for each group of common triggers, corresponding to the plunge direction of the plane. Figure 2.64a shows the epicentre of a theoretical source, located at depth of 20 km, roughly corresponding to the epicentre and the depth of the tremor source reported in *Nadeau and Dolenc* (2005); the distribution of the theoretical travel times, calculated using this theoretical source, are shown as the surface in Figure 2.64b and black circles in Figure 2.64c. In these figures, the best fit plane obtained taking into account only the 13 points corresponding to the stations is shown as a grid.

The values for "N" and "E" were chosen to be 7 and 10, respectively, as representing a good trade-off between consistency of the time distribution of the common triggers with the distribution of the stations, and high number of remaining groups of common triggers.

28.3 Detection Results

By applying the detection procedure on the 5 lists of common triggers, we found 161 "events" that can be divided into two groups. The first consists of 17 events with impulsive onsets, clear P- and S-waves arrivals and a broad spectrum (5-15 Hz) (Figure 2.65a,b). Based on these features we consider them to be earthquakes (most of them are reported in the Northern California Earthquake catalog). The second group has 144 events. They have emergent onsets, low overall amplitudes, generally higher amplitudes on the horizontal components than on the vertical, and a narrow spectrum enriched in low frequencies (below 8 Hz; Figure 2.65c,d).

While the azimuths, from the plunges of the best fit planes, for the first group are scattered, those of the second group are nearly constant (Figure 2.66a,b). Their direction is roughly consistent with the location of the tremor source reported in *Nadeau and Dolenc* (2005).

28.4 Conclusion

By developing an effective detection procedure, we were able to find two different groups of events in the seismic signal recorded during 48 episodes of NVT. The first family are earthquakes, most of which are reported in the NCSN catalog. The second was composed of tremor pulses, characterised by spectral content similar to the NVT and constant at all the stations, and by steady azimuth of seismic wave propagation, consistent with the location of the NVT source.

28.5 References

Nadeau, R.M., and D. Dolenc, Nonvolcanic tremors deep beneath the San Andreas fault, *Science*, *307*, doi:10.1126/science.1107142, 2005.

Obara, K., Nonvolcanic deep tremor associated with subduction in southwest Japan, *Science*, *296*, 1679-1681, 2002.

Shelly, D.R., Beroza, G.C., Ide, S., and S. Nakamula, Low-frequency earthquakes in Shikoku, Japan, and their relationship to episodic tremor and slip, *Nature*, *442*, 188-191, 2006.

Shelly, D.R., Beroza, G.C., and S. Ide, Non-volcanic tremor and low-frequency earthquake swarms, *Nature*, *446*, 305, 2007.

Schwartz, S.Y., and J.M. Rokosky, Slow slip events and seismic tremor at circum-Pacific subduction zones, *Rev. Geophys.*, *45*, RG3004, doi:10.1029/2006RG000208, 2007.

Withers, M., Aster, R., Young, C., Beiriger, J., Harris, M., Moore, S., and J. Trujillo, A comparison of select trigger algorithms for automated global seismic phase and event detection. *Bull. Seism. Soc. Am.*, *88*, 95-10, 1998.